Video Article

Experimental Methods for Investigation of Shape Memory Based Elastocaloric Cooling Processes and Model Validation

Marvin Schmidt[1,2], Johannes Ullrich[2], André Wieczorek[3], Jan Frenzel[3], Gunther Eggeler[3], Andreas Schütze[1], Stefan Seelecke[2]

[1]Lab for Measurement Technology, Saarland University

[2]Intelligent Material Systems Lab, Saarland University

[3]Lab for Material Science, Ruhr Universität Bochum

Correspondence to: Stefan Seelecke at stefan.seelecke@mmsl.uni-saarland.de

URL: http://www.jove.com/video/53626
DOI: doi:10.3791/53626

Keywords: Engineering, Issue 111, Elastocaloric cooling, Phase transformation, Shape memory alloy, Process optimization, Scientific test rig, Latent heats, Solid state cooling, Thermomechanically coupled model

Date Published: 5/2/2016

Citation: Schmidt, M., Ullrich, J., Wieczorek, A., Frenzel, J., Eggeler, G., Schütze, A., Seelecke, S. Experimental Methods for Investigation of Shape Memory Based Elastocaloric Cooling Processes and Model Validation. *J. Vis. Exp.* (111), e53626, doi:10.3791/53626 (2016).

Abstract

Shape Memory Alloys (SMA) using elastocaloric cooling processes have the potential to be an environmentally friendly alternative to the conventional vapor compression based cooling process. Nickel-Titanium (Ni-Ti) based alloy systems, especially, show large elastocaloric effects. Furthermore, exhibit large latent heats which is a necessary material property for the development of an efficient solid-state based cooling process. A scientific test rig has been designed to investigate these processes and the elastocaloric effects in SMAs. The realized test rig enables independent control of an SMA's mechanical loading and unloading cycles, as well as conductive heat transfer between SMA cooling elements and a heat source/sink. The test rig is equipped with a comprehensive monitoring system capable of synchronized measurements of mechanical and thermal parameters. In addition to determining the process-dependent mechanical work, the system also enables measurement of thermal caloric aspects of the elastocaloric cooling effect through use of a high-performance infrared camera. This combination is of particular interest, because it allows illustrations of localization and rate effects — both important for efficient heat transfer from the medium to be cooled.

The work presented describes an experimental method to identify elastocaloric material properties in different materials and sample geometries. Furthermore, the test rig is used to investigate different cooling process variations. The introduced analysis methods enable a differentiated consideration of material, process and related boundary condition influences on the process efficiency. The comparison of the experimental data with the simulation results (of a thermomechanically coupled finite element model) allows for better understanding of the underlying physics of the elastocaloric effect. In addition, the experimental results, as well as the findings based on the simulation results, are used to improve the material properties.

Video Link

The video component of this article can be found at http://www.jove.com/video/53626/

Introduction

Solid state cooling processes based on ferroic materials have potential to be environmentally friendly alternatives to the conventional vapor compression based process. Ferroic materials may exhibit magnetocaloric, electrocaloric and elastocaloric effects [1,2], as well as combinations of these effects, which are described as multicaloric material behavior [3]. The different caloric effects in ferroic materials are currently being investigated as part of the German Science Foundation (DFG) Priority program SPP 1599 "Caloric Effects in Ferroic Materials: New Concepts for Cooling" [4]. Shape Memory Alloys (SMA) which are investigated within this program show large elastocaloric effects, in particular Ni-Ti based alloys due to their large latent heats [5]. The strain-induced phase transformation at high strain rates leads to significant temperature changes of the SMA, as shown in **Figure 1**. The adiabatic, exothermic phase transformation from austenite to martensite increases the SMA temperature. The endothermic transformation from martensite to austenite leads to a significant temperature decrease. These elastocaloric material properties can be used for solid-state cooling processes by applying a suitable mechanical loading and unloading cycle. **Figure 2** shows a typical elastocaloric cooling cycle, following the Brayton cycle. The heat transfer between the heat source and the cold, unloaded SMA take place at low temperature levels. In the next phase, the SMA is in a contact-free state and the fast, adiabatic loading leads to a significant temperature increase of the SMA. The subsequent heat transfer between the hot SMA and the heat sink take place at constant strain of the SMA. Upon completion of the heat transfer, fast, adiabatic unloading leads to a significant temperature drop of the SMA below the temperature of the heat source, whereupon the next cooling cycle and the heat transfer with the heat source can start. The efficiency of the elastocaloric cooling process depends on the required mechanical work and the absorbed heat.

First, experiments monitoring the temperature field during tensile tests were performed by Shaw *et al.* [6,7], with the objective to investigate the formation of local temperature peaks during tensile tests of SMA strips and wires at different rates. The applied experimental method combined the measurement of the mechanical parameters (stress, strain and strain rate) with simultaneous acquisition of temperature fields by means of thermographic measurements. During loading and unloading of a SMA specimen with a tensile testing machine, an infrared (IR) camera was

used to acquire IR images of the SMA sample. This technique enables the investigation of the strain rate dependent formation of temperature peaks. The measurement of the temperature distribution on the sample is very important for the investigation of the elastocaloric effects and the determination of the cooling properties of the material. A local temperature measurement — by applying a contacting temperature measurement — is not sufficient in order to characterize the cooling properties of the material. A measurement of the temperature field was also used by Cui *et al.* [8] for the study of elastocaloric effects in Ni-Ti wires. Furthermore, Ossmer *et al.* [9,10] showed that thermographic temperature measurements are also suitable for the investigation of elastocaloric effects in Ni-Ti based thin films, which required high frame rates of the IR camera for the investigation of adiabatic phase transformations at high strain rates. This technique allows for the investigation of elastocaloric quantities and the homogeneity of the temperature profile, which has a significant influence on the solid-state based heat transfer and the efficiency of elastocaloric processes.

The cooling efficiency of the material can be determined by calculating the required work based on the stress/strain measurements as well as the heat (which can be determined taking into account the temperature change and the heat capacity of the material). However, the experimental method does not enable the investigation of the elastocaloric material under process condition. This includes a heat transfer between the SMA and a heat source, which has a significant influence on the efficiency of the cooling effect.

The material characterization of cooling process conditions and the investigation of elastocaloric cooling processes require a test rig enabling solid-state based heat transfer, which cannot be investigated by any existing commercial system. To this end, a novel testing platform has been developed. The test rig is set up in two levels as shown in **Figure 3**. The upper level allows for basic elastocaloric material characterization and initial training procedures, similar to the previously described method (see **Figure 4**). The setup is equipped with a linear direct drive capable of loading and unloading the SMA at strain rates up to 1 sec^{-1} (see **Figure 5**). The linear direct drive enables the investigation of samples with a cross section of up to 1.8 mm^2, while the typical sample length is 90 mm. The advantage of a linear direct drive is the high velocity and the high acceleration — in contrast to ball screw drives which are typically used for tensile tests. Furthermore, a load cell, as well as the integrated position measurement system of the linear drive, provides mechanical measurement data. A high-resolution IR camera (1,280 x 1,024 pixels) is used to measure the temperature profile of the SMA with up to 400 Hz (in the required temperature range). The use of a microscope lens with a resolution of 15 µm/pixel enables the investigation of local temperature effects. The lower level of the test rig contains a mechanism that allows for alternating conductive heat transfer between the SMA and the heat source/heat sink (see **Figures 6** and **7**). The linear direct drive in the lower level switches between the heat source to the SMA and from the SMA to the heat sink, whereas a pneumatic cylinder lifts and lowers the heat source/sink (see **Figure 8**). Each actuator can be controlled independently allowing for investigation of different cooling process variations. The comprehensive measurement system enables measurements of mechanical parameters: actuator position, actuator velocity, SMA loading force, contact force between SMA and heat source/sink during heat transfer as well as thermal parameters (*i.e.*, temperatures inside the heat source/sink, temperature distribution on the surface of the SMA and the heat source/sink). A more detailed description of the scientific testing platform is given in Schmidt *et al.* [11].

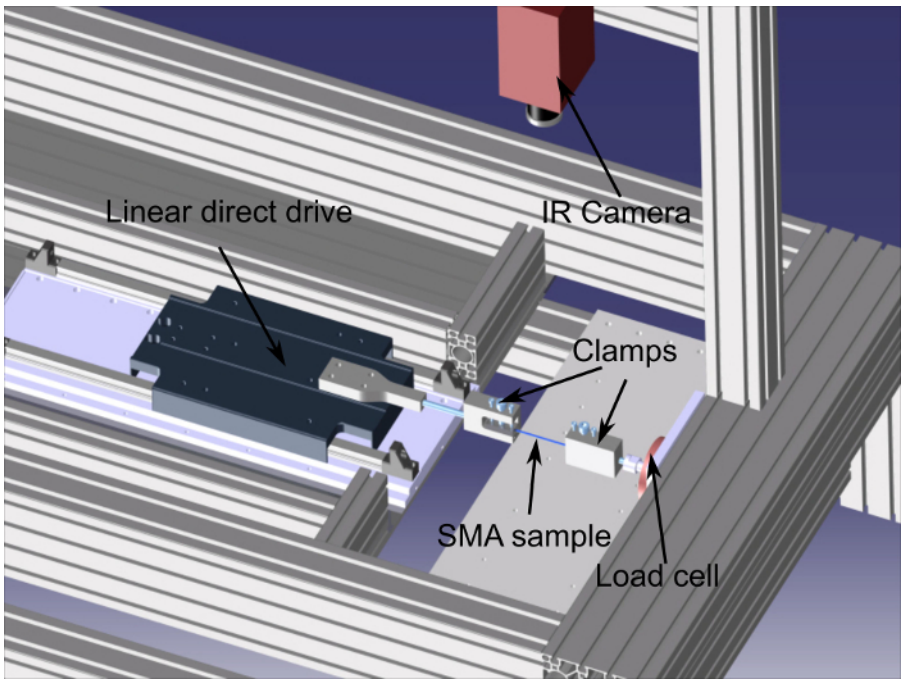

Figure 5. Scheme of the upper level of the test rig. A linear direct drive for loading and unloading of the SMA sample with integrated position measurement system; a load cell for measuring of tensile forces, as well as a high-resolution IR camera (1,280 x 1,024 pixels) for temperature profile acquisitions.

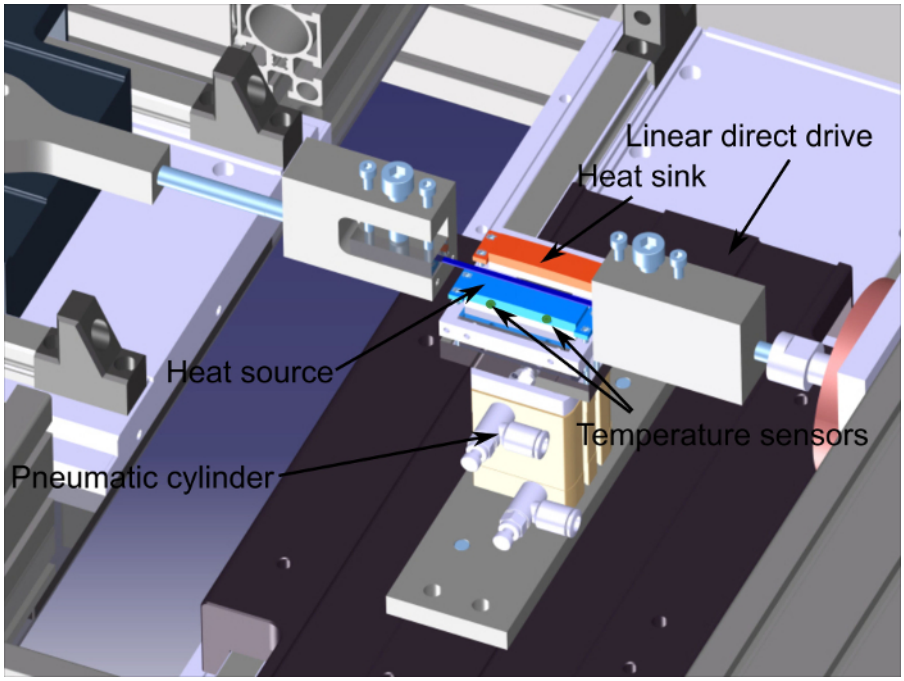

Figure 7. Scheme of the lower level of the test rig. A linear direct drive for switching between heat sink and heat source; a pneumatic cylinder to make contact between the SMA sample and the heat source/sink; temperature sensors have been integrated in the heat sink/source to measure the core temperature of the blocks. A compression load cell for measuring the contact force between the SMA and the heat source/sink is integrated in the heat transfer mechanism and not visible in this scheme.

The test rig allows for the investigation of different alloy compositions and sample sizes as well as geometries (ribbons, wires). Furthermore, the setup enables comprehensive investigations of elastocaloric materials and cooling processes. The previously described experiments can be performed and the execution will be described step-by-step in the protocol section of this manuscript.

Material stabilization:

Stable material behavior is important for the use of elastocaloric materials in cooling systems. To this end, a mechanical stabilization procedure is applied. During this procedure the material passes mechanical loading and unloading cycles and performs a phase transformation from austenite to martensite. The material stabilization shows a strong rate dependency. High loading rates lead to a temperature change of the material, which is caused by the latent heat of the phase transformation. This temperature change has a similar influence on the material stabilization, as do mechanical training cycles at various temperatures [12-15]. In addition to the well-known mechanical [13] and caloric [16] stabilization, a thermal material stabilization can be observed with the designed setup by applying thermography [17].

Material characterization:

After an initial mechanical training procedure, the material shows stable mechanical, thermal and caloric behavior allowing the elastocaloric material properties to be characterized. Therefore, mechanical cycling at different rates is performed whereas, in contrast to the training procedure, the elastocaloric characterization includes a holding phase after loading and unloading. For the duration of the holding phase the SMA strain is kept constant until an ambient temperature level is reached again. This type of experiment is required in order to determine the lowest achievable temperature after unloading, starting from ambient temperature levels, as well as the material efficiency. Rate dependent formation of local temperature peaks can be observed, with higher rates leading to an increasingly homogeneous temperature distribution. Furthermore, by increasing the strain rate the temperature change equally increases until adiabatic conditions are achieved. The material efficiency can be determined by calculating the required mechanical work, based on a force-displacement diagram of an adiabatic experiment, as well as the absorbable heat, based on the mean temperature change of the material during unloading and the heat capacity of the sample.

Elastocaloric cooling process:

The investigation of the cooling efficiency of SMAs under process conditions requires the heat transfer between the SMA cooling medium and a heat source, as well as a heat sink. For this purpose, the SMA is in contact with a solid-state heat source (following adiabatic unloading) and a heat sink (following adiabatic loading). The efficiency of the process strongly depends on the process control and the thermal boundary conditions. The comprehensive investigation of the cooling process requires a variation of the control parameters in order to determine the most efficient process control. The individual influence of the parameters (contact time, SMA strain, SMA strain rate, contact phase (contact during the loading/unloading phase or following) and contact force) on the process performance has to be investigated. Furthermore, the influence of the changing thermal boundary condition by increasing number of cooling cycles has to be taken into account.

Model validation:

The development of a thermomechanically coupled material model, capable of reproducing the mechanical and thermal material behavior during cooling cycle, is crucial for the development of a novel cooling technology. The model allows for material and process optimization by reduced experimental and material development effort. The validation requires an initial isothermal tensile test of a stabilized material to generate the

required mechanical material input data (elastic modulus of the austenite and the martensite phase, the width of the mechanical hysteresis as well as the transformation strain). The validation of the model takes place on the basis of tensile tests at different rates. The required caloric input data for the model can be determined by differential scanning calorimetry (DSC) following the mechanical experiments. The DSC measurements have to be performed after the mechanical test in order to measure the caloric material properties of a stabilized sample.

Protocol

1. Sample Preparation

1. Measure the SMA ribbon with calipers and determine the cross section of the sample.
2. Prepare the sample for IR measurements by coating the ribbon with a thin layer of high emissivity (ε=0.96) paint.
   Caution: The paint is classified as an irritant. Gloves, safety glasses and mouth protection must be worn during the processing of the paint.

2. Material Stabilization (Training)

Note: Initial mechanical cycling leads to a mechanical and thermal material stabilization. The investigation of the stabilization effect, and the training procedure itself, requires the use of the actuator and the sensors mounted in the upper level of the test rig as well as the IR camera.

1. Start motor controller program and check the loaded settings. Change the settings to position mode and command mode. Verify the motor is in active mode.
2. Set the target position in the motor controller program to 0 µm and click on the "operation enable" button — at this position the distance between the clamps is 90 mm.
3. Place the sample between clamps of the experimental setup and use a special designed alignment tool to align the sample.
4. Tighten clamps using a mounting aid in order to avoid bending load on load cell and sample. Use a torque wrench for tightening the screws to ensure a reproducible clamping force (tightening torque: 20 Nm).
5. Check current motor position and make sure that the motor is at start position (0 µm).
6. Start the IR camera software and load the calibration for a 50 mm lens combined with a close-up lens. Choose an image size of 1,280 x 100 pixels and a temperature range of -20 °C to 50 °C. Position the camera by using the motor focus unit and confirm the whole sample is in the field of view of the camera.
   Note: The IR camera, in combination with the chosen lens system, has a focal length (f) of 50 mm, an aperture of f/2 and a minimum pixel size of 60 µm at a working distance of 200 mm.
7. Open the control program for training and material characterization and set the control parameters (displacement, velocity, holding time, maximum and minimum force, number of cycles and camera frame rate).
   1. Set the start position (0 µm) and choose the target position (4,500 µm) so that the material undergoes a complete phase transformation.
   2. Set the linear direct drive velocity (velocity loading/ unloading) to meet the desired strain rate. Select a strain rate of 5 x 10^{-4} sec^{-1} (actuator velocity of 45 µm/sec) for cooling process related training.
      1. Determine the linear direct drive velocity (v) based on the chosen strain rate ($\dot{\varepsilon}$) and the initial sample length (l_0) of 90 mm ($v = \dot{\varepsilon} \cdot l_0$)
   3. Set the holding time to 0 sec.
   4. Set the number of cycles to 1 for the first cycle with a new sample.
   5. Set the sample-specific minimum and maximum force level to avoid compressive load and tensile overload (minimum load 1 MPa, maximum load 800 MPa).
   6. Choose an IR camera acquisition rate of 50 msec/frame (20 frames per second).
   7. Click on the start button to load the settings.
8. Open the IR camera software, choose a file name and allocate 5,000 frames.
   1. Switch from internal to external trigger source and start the data acquisition mode.
9. Open the control program and press the start experiment button.
10. Data visualization
    1. Once the experiment is finished, load the data into the data processing software and visualize it in terms of force/displacement, stress/strain, force/time and position/time diagrams.
    2. Load the IR data into the IR camera software and evaluate the time resolved temperature profiles. Define a measurement area which covers the surface of the SMA ribbon and plot the mean maximum and minimum temperature of the sample vs. time.
11. Repeat steps 2.6 to 2.9 until the material shows stable mechanical behavior and adapt the start position to compensate for residual strains.
    1. After the first 10 cycles, increase the number of cycles per experiment to 10 and proceed with the experiments until stable material behavior is reached.

3. Material Characterization

Note: The material characterization requires the use of the actuator and the sensors mounted in the upper level of the test rig as well as the IR camera. During the characterization procedure the sample is loaded and unloaded at different rates while performing a holding period after loading and unloading.

1. If the SMA ribbon has been unclamped and the control system of the test rig has been switched off after the training, repeat steps 2.1 to 2.6 and clamp the sample again. If this was not the case, proceed as follows.
2. Open the control program for training and material characterization and set the control parameters (displacement, velocity, holding time, number of cycles and camera frame rate).
    1. Set the start position so that the sample is under zero load and set the target position equivalent to the target position of the training (4,500 µm).
    2. Set the linear direct drive velocity (velocity loading/unloading) to meet the desired strain rate. Choose a strain rate of 1 x 10^{-1} sec^{-1} (actuator velocity of 9,000 µm/sec) which leads to an adiabatic phase transformation for samples with a cross section of 0.75 mm x 1.4 mm or larger.
    3. Set the holding time to 180 sec, which is sufficient for the sample to reach the initial temperature level.
    Note: The holding time has to be verified after the experiment by calculating a thermal equilibration time constant (τ) and a holding time smaller than 4 x τ has to be increased before the next characterization experiment starts.
    4. Set the number of cycles to 1.
    5. Set the sample-specific minimum and maximum force level to avoid compressive load and tensile overload (minimum load 1 MPa, maximum load 800 MPa).
    6. Choose an IR camera acquisition rate of 5 msec/frame (200 frames per second).
    7. Click on the start button to load the settings.
3. Open the IR camera software, choose a file name and allocate 80,000 frames.
    1. Switch from internal to external trigger source and start the data acquisition mode.
4. Open the control program and press the start experiment button.
5. Load the IR data into the IR camera software. Plot mean maximum and minimum sample temperatures vs. time. Export the data and calculate the thermal equilibration time constant with the data processing software [10,11].
6. Adapt the holding time, if necessary, based on the calculated thermal equilibration time constant.
7. Repeat steps 3.2 to 3.5 and vary the strain rate from 5 x 10^{-5} sec^{-1} to 1 x 10^{-1} sec^{-1}, as well as the strain from 2% to a maximum strain of 5% (maximum strain is equivalent to the maximum strain during training).
8. Investigation of local temperature peaks:
Note: The material shows a rate-dependent localization effect of the elastocaloric effect. Careful study of these effects requires a high special resolution of the SMA temperature profile. For this purpose, the lens of the IR Camera has to be replaced by a microscope lens. The microscope lens has an aperture of 3.0, a magnification of 1X and a pixel size of 15 µm at a working distance of 195 mm.
    1. Switch the light off, remove all heat sources from the field of view of the IR camera and change the lens.
    2. Change the camera calibration settings and load a microscope lens calibration within the temperature range of 20 °C to 50 °C and an image size of 500 x 250 pixels. Use the motor focus unit to focus the sample.
    3. Perform a tensile test at a strain rate of 1 x 10^{-1} sec^{-1} (9,000 µm/sec), follow the steps described in section 2: Material stabilization.
9. Data Visualization
    1. Load the mechanical data into the data processing software and visualize it in terms of force/displacement, stress/strain, force/time and position/time diagrams.
    2. Load the IR data into the IR camera software and evaluate the time resolved temperature profiles. Define a measurement area which covers the surface of the SMA ribbon and plot the mean maximum and minimum temperature of the sample vs. time.

4. Elastocaloric Cooling Process

Note: The investigation of elastocaloric cooling processes requires the use of actuators and sensors in the upper and lower level of the setup as well as the IR camera. These experiments include a variation of the control parameters in order to optimize the process performance.

1. If the SMA ribbon has been unclamped and the test rig has been switched off after the material characterization, repeat steps 2.1 to 2.5 and clamp the sample again. If this was not the case, proceed as follows.
2. Start the IR camera software and load the calibration for the 50 mm lens with close-up lens. Choose an image size of 1,280 x 1,024 pixels and a temperature range of -20 °C to 50 °C. Position the camera by using the motor focus unit and make sure that the entire sample is in the field of view of the camera.
Note: The IR camera in combination with the chosen lens system has a focal length (f) of 50 mm, an aperture of f/2 and a minimum pixel size of 60 µm at a working distance of 200 mm.
3. Open the control program for elastocaloric cooling processes and set the control parameters (displacement of linear direct drive one (upper level), velocity of linear direct drive one and two, contact time, maximum and minimum force, contact phase, number of cycles and camera frame rate).
    1. Set the start position of the linear direct drive for SMA loading and unloading, so that the sample is under zero load and set the target position equivalent to the target position of the training (4,500 µm).
    2. Set the velocity (velocity loading/unloading) of the linear direct drive for loading and unloading of the SMA to meet a strain rate of 1 x 10^{-1} sec^{-1} (9,000 µm/sec). Set the velocity of the linear direct drive in the lower level of the setup to 100 mm/sec.
    3. Set the contact time to 6 sec.

Note: The contact time determines the duration of the heat transfer and can be set to any value above 10 msec.
4. Choose the contact after loading/unloading mode.
Note: The contact phase influences whether the loading and unloading is adiabatic (contact after loading/unloading) or combined with a heat transfer to the heat sink/source (contact during loading/unloading).
5. Set the number of cycles to 40.
6. Set the sample-specific minimum and maximum force level to avoid compressive load and tensile overload (minimum load 1 MPa, maximum load 800 MPa).
7. Choose an IR camera acquisition rate of 20 msec/frame (50 frames per second). Click on the start button to load the settings.

4. Open the IR camera software, choose a file name and allocate 50000 frames. Switch from internal to external trigger source and start the data acquisition mode.
5. Open the control program and press the start experiment button.
6. Data visualization
1. Once the experiment is finished load the data into the data processing software and visualize the following data: force/displacement, stress/strain, temperature/time (temperature of the heat sink/source), force/time, contact force/ time and position of the linear actuators/ time.
2. Load the IR data into the IR camera software and evaluate the time resolved temperature profiles. Define three measurement areas which cover the surface of the SMA sample as well as the surface of the heat sink and the heat source. Export the time resolved mean, maximum and minimum temperature data of the defined measurement areas and load them into the data processing software.
3. Visualize the IR data in a temperature/time diagram.

7. Repeat the experiment under variation of the parameters: strain, contact time and contact phase.

5. Model Validation

Note: The validation of thermo-mechanically coupled material models requires experiments adhering to material stabilization or material characterization. Use a Ni-Ti wire with a cross section of 0.6 mm to perform the experimental investigations.

1. Perform an isothermal tensile test at a strain rate of 5×10^{-5} sec^{-1} and a strain of 5%, proceed by performing the steps described in Section 2.
2. Once the experiment is finished, load the data into the data processing software and visualize the stress/strain measurement. Calculate the elastic modulus of the austenite and the martensite phase, the transformation strain as well as the width of the hysteresis. The aforementioned data function as mechanical input data for the model [7].
3. Perform further tensile tests at strain rates of 1×10^{-4} sec^{-1}, 5×10^{-4} sec^{-1}, 1×10^{-3} sec^{-1}, 5×10^{-3} sec^{-1}, 1×10^{-2} sec^{-1}, 5×10^{-2} sec^{-1}, 1×10^{-1} sec^{-1} to generate validation data for the model.
4. If the experiments are completed take the sample out of the test system and perform a differential scanning calorimetric measurement (DSC) [18] to determine the caloric material properties (latent heats of the phase transformation and specific heat capacity of the material) of the stabilized material.
Note: The DSC measurements provide caloric input data for the thermo-mechanically coupled model.
5. Start the simulation of the tensile tests described in step 5.3.
1. Implement custom model for shape memory alloys into commercially available finite element software:
1. Select *Geometry* node and choose *Interval* to draw 1D wire geometry.
2. Select *Parameters* node to define model parameters identified from mechanical tests in step 5.2.
3. Right-click *Definitions* node and select *Variables* to create a *Variables* node. Select *Variables* node and define algorithm for determining the transition probabilities derived from statistical thermodynamics [19].
4. Select *Add Physics* and add *Coefficient Form PDE* or *General Form PDE* to define set of one-dimensional partial differential equations describing the behavior of superelastic Shape Memory Alloy, consisting of the stationary momentum balance, the balance of internal energy and kinetic equations of phase transformation [20].

2. Select *Initial Values* sub-node to set the initial temperature of the wire to the environment temperature.
1. Select *Dirichlet Boundary Condition* to prescribe mechanical boundary conditions for applying a strain following the experimental procedure described in section 2, for the strain-rates in step 5.3, constraining the displacement of one end of the wire and prescribing the displacement of the other end.
2. Select *Dirichlet Boundary Condition* to set thermal boundary conditions to constant temperature because of the massive clamps compared to the thin wire.
Note: Standard settings of the finite element software do not lead to a converging solution.
3. Select sub-nodes of *Solver Configuration* to modify standard settings (*e.g.*, absolute and relative tolerances and damping coefficient of the nonlinear, iterative Newton-Raphson solver) and click "Compute" to run solver.

6. Data Analysis
1. Load the experimental and simulation results into the data analysis software and visualize the mechanical and thermal data.
2. Compare the experimental and simulation results, respective mechanical (stress/strain response) and thermal (special resolved temperature evolution of the sample) material behavior.

Representative Results

Material stabilization (Training):

Figure 9 shows a stress/strain diagram of 50 training cycles. The investigated sample is a Ni-Ti ribbon with a cross section of A = 1.45 mm^2. The applied strain rate of 1 x 10^{-3} sec^{-1} leads to a mean temperature increase of ΔT = 12.2 K. The temperature increase has a significant influence on the stabilization effect [12-14]; in addition to the mechanical stabilization, a thermal stabilization can be observed as well. **Movie 1** shows the temperature distribution on the sample during the first three training cycles, the frame rate is five times higher as the real time measurement. The experiment was stopped after each cycle and restarted as soon as the sample reached ambient temperature. A homogenization of the elastocaloric effect is observed however the intensity of the temperature peaks decreases by increasing number of cycles.

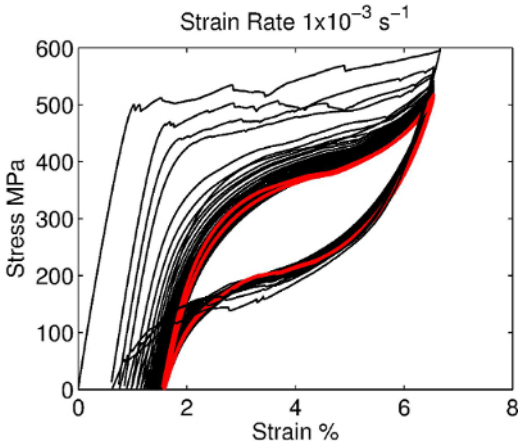

Figure 9. Mechanical stabilization of a binary Ni-Ti ribbon during training. Stress/strain diagram of 50 training cycles at a strain rate of 1 x 10^{-3} sec^{-1}.

Material characterization:

The results of an elastocaloric material characterization of a NiTiCuV ribbon (A = 1.07 mm^2) are shown in **Figure 10**. The stress/strain diagram in **Figure 10 (a)** shows that increasing strain rates lead to increasing hysteresis width [7,12,21]. This correlation is a result of the temperature change during the phase transformation, which is also shown in the ΔT-strain rate diagram (**Figure 10 (b)**). Furthermore, the diagram shows that at strain rates higher than 5 x 10^{-2} sec^{-1} there is no further increase of the temperature change. The stagnation of the temperature change indicates that the adiabatic limit is reached, which can also be derived from the stagnation of the temperature related stress increase (shown in the stress-strain diagram). Furthermore, the small deviation between the mean and maximum temperature change at high rates shows that the material transforms almost homogeneously. The comparison of the IR videos acquired during the experiments performed at a strain rate of 1 x 10^{-3} sec^{-1} (see **Movie 2** (loading) and **Movie 3** (unloading)) and at a strain rate of 1 x 10^{-1} sec^{-1} (see **Movie 4** (loading, 10 times slower) and **Movie 5** (unloading 10 times slower)) shows the homogenization of the elastocaloric effect by increasing strain rates.

Based on the material characterization, the efficiency of the material can be determined. The work of an adiabatic loading and unloading cycle at a strain rate of 1 x 10^{-1} sec^{-1} is equivalent to the areas in the force-deflection diagram in **Figure 11**. The red area shows the non-recoverable work of the hysteresis which is taken into account for the determination of the Coefficient of Performance (COP) of the material. The heat is calculated based on the mean negative temperature change of 20 K and the heat capacity of the sample, whereas the heat capacity can be determined by taking in to account the specific heat capacity (cp = 0.46 J/(kg K)), the density (ρ = 7,340 kg/cm^3) and the volume of the sample. The resulting COP of 7 is the quotient of absorbed heat and mechanical work. A graphical method to determine the efficiency of elastocaloric cooling processes based on the thermodynamic analysis of cooling cycles is described in Schmidt *et al.* [22]

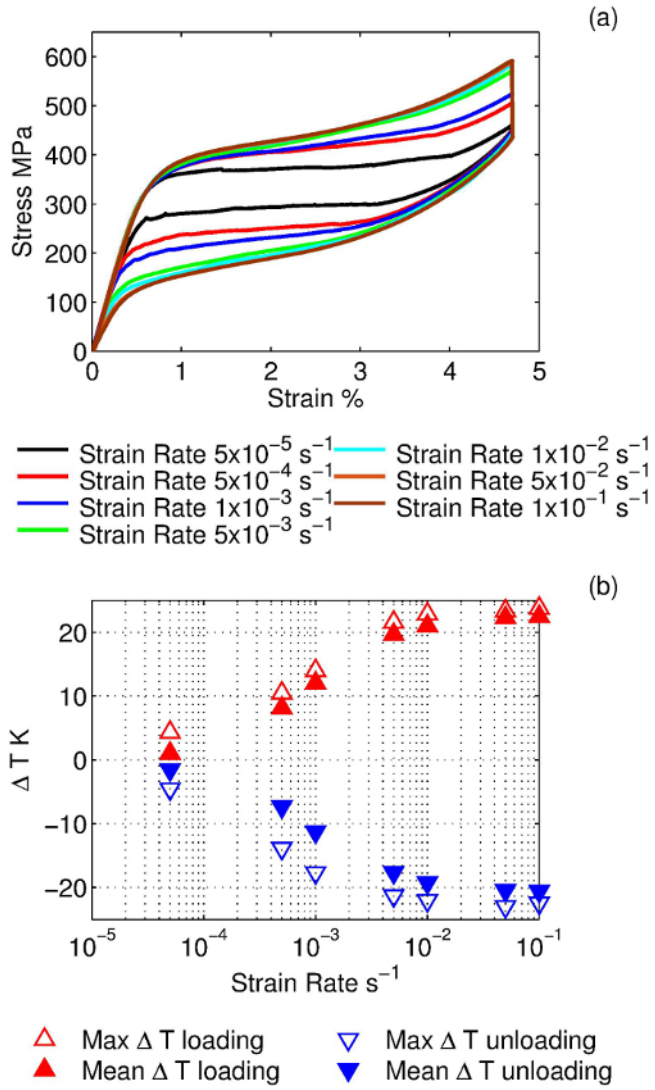

Figure 10. Material characterization. Rate-dependent stress/strain diagram (**a**) and ΔT/strain rate diagram showing minimum, maximum and mean SMA temperature change (**b**) of a NiTiCuV ribbon. The strain was kept constant for 150 sec after loading and unloading.

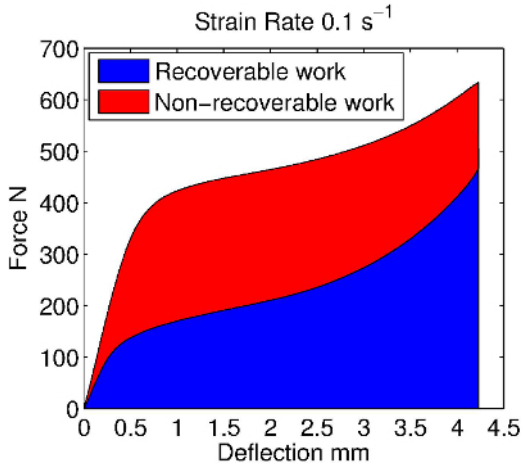

Figure 11. Work. Force/deflection diagram of a NiTiCuV ribbon (A = 1.07 mm^2) during an adiabatic loading and unloading cycle. The deflection was kept constant for 150 sec after loading and unloading. The work is equivalent to the areas in the diagram whereas the work during unloading could potentially be recovered.

Cooling process:

The force deflection diagram in **Figure 12 (a)** shows the mechanical behavior of the previously characterized NiTiCuV sample during 40 cooling cycles. The contact time between the SMA and the heat source/sink was set to 6 sec and the strain rate was set to 1 x 10^{-1} sec^{-1}. The temperature-time diagram in **Figure 12 (b)** shows the temperature increase of the heat sink and the temperature decrease of the heat source during the 40 cooling cycles, which changes the thermal boundary conditions of the process. Furthermore, the influence of the boundary conditions to the mechanical and the thermal material behavior can be observed. The IR video (**Movie 6**) shows that by increasing the number of cycles the minimum and maximum temperature change of the material decreases This is also reflected in the decrease of the hysteresis width (see **Figure 12 (a)**). After the first cycle, an inhomogeneous temperature profile arises because the heat sink/source does not contact the whole SMA ribbon (see **Movie 6**). The significant different temperature profile of the SMA after the first cycle leads to a lower transformation strain in the second cycle (see **Figure 12 (a)**). The COP of the process strongly depends on the temperature of the heat sink and the heat source as shown in **Figure 13**. The increasing temperature difference between heat sink and heat source leads to a decreasing COP, which is related to the decreasing temperature difference between the heat source and the SMA. The COP is calculated based on the non-recoverable work (see **Figure 10**) and the absorbed heat during contact between the SMA and the heat source. The absorbed heat is determined by taking into account the heat capacity of the SMA and the mean temperature change of the SMA during contact to the heat source. The cooling power per unit surface area of the process shows an equivalent trend (see **Figure 14**). The cooling power per unit surface area can be calculated based on the absorbed heat per cycle, the cycle time of 13.1 sec and the surface area of the sample in contact with the heat source (8.4 x 10^{-6} m^2). This example of a SMA based cooling process demonstrates that the material shows a different behavior under process conditions in comparison to material characterization. The heat transfer and the process control influence the cooling performance of the material and have to be taken into account for the validation of elastocaloric materials.

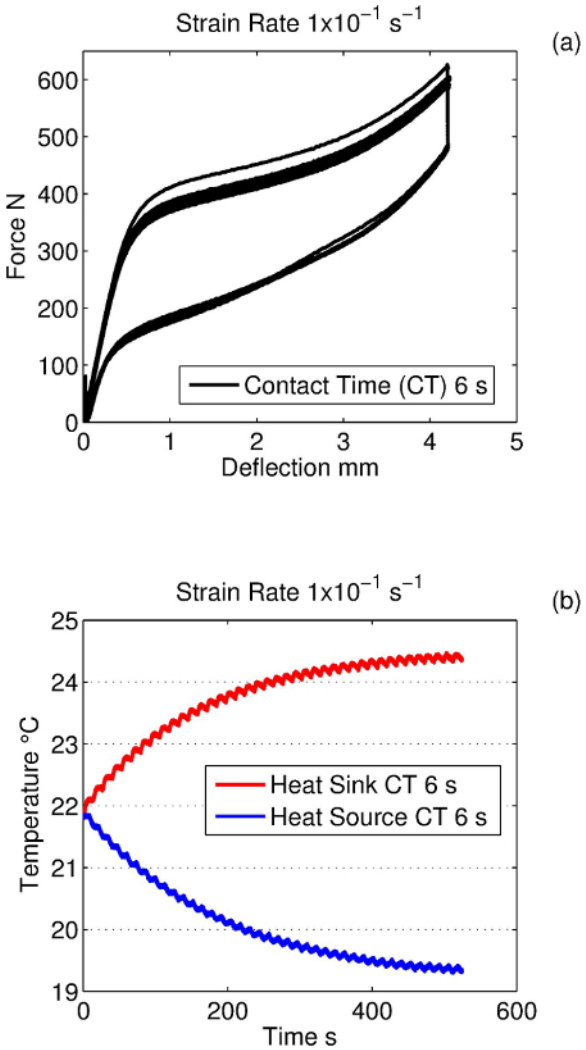

Figure 12. Cooling process. Force/deflection diagram (**a**) and temperature/time diagram (**b**) of a 40 cycle cooling process with a NiTiCuV sample (A = 1.07 mm^2) and a contact time of 6 sec.

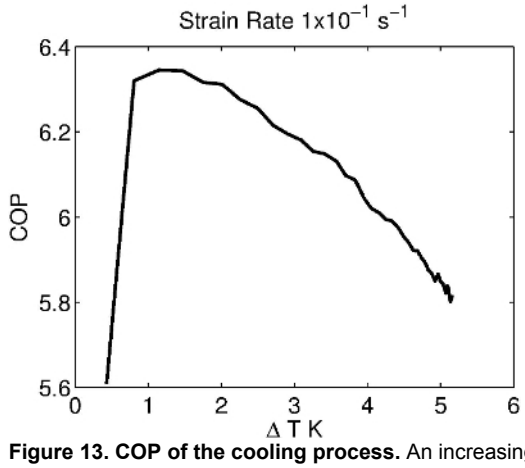

Figure 13. COP of the cooling process. An increasing number of cooling cycles leads to a decreasing COP and an increasing temperature difference between heat sink and heat source.

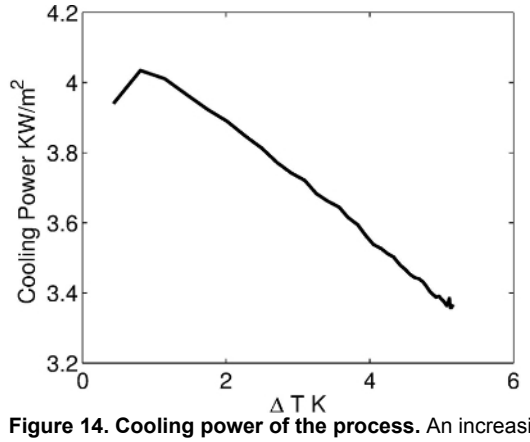

Figure 14. Cooling power of the process. An increasing number of cooling cycles leads to a decrease of the cooling power per unit surface area and an increasing temperature difference between heat sink and heat source.

Model validation:

Figure 15 (see also **Movie 7**) shows the comparison between experiment and simulation of a tensile test performed at a strain rate of 1 x 10^{-3} sec^{-1}. The comparative sample was a Ni-Ti wire with a diameter of 0.6 mm and a clamping length of 90 mm. The underlying model of the simulation is a modification of the thermomechanically coupled Müller-Achenbach-Seelecke (MAS) model [23,24,19]. The model was extended to allow for the simulation of localized phase transformation and inhomogeneous temperature distribution. The comparison between the experimental results (see **Movie 7 (a)**) and the simulation (see **Movie 7 (b)**) shows that the model is able to reproduce the mechanical as well as the thermal material behavior. The simulated temperature fields show localized temperature peaks and the intensity of the peaks show a good correlation with the experiment. Furthermore, the timing of the temperature peak formation and the resulting stress decrease shows good agreement. The applied model approach is not only limited to the simulation of the material behavior at tensile load, also a bending load can be simulated [25]. The physically motivated model allows for detailed analysis of the underlying mechanisms and supports process and material optimization by reducing experimental and material development effort.

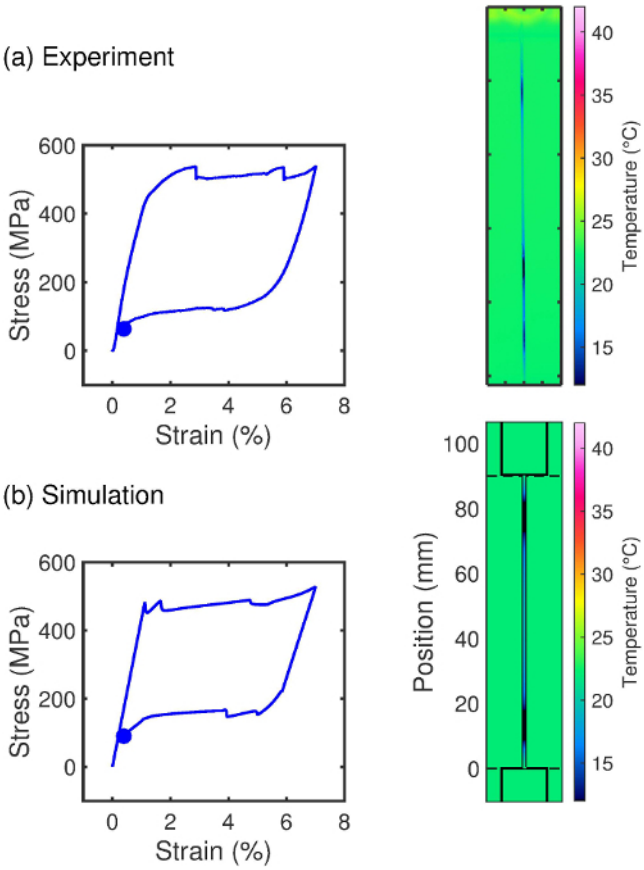

Figure 15. Comparison between experiment (a) and simulation (b) results of a Ni-Ti wire with a diameter of 0.6 mm (A = 0.2734 mm^2). The validation experiment is a tensile test at a strain rate of 1 x 10^{-3} sec^{-1}.

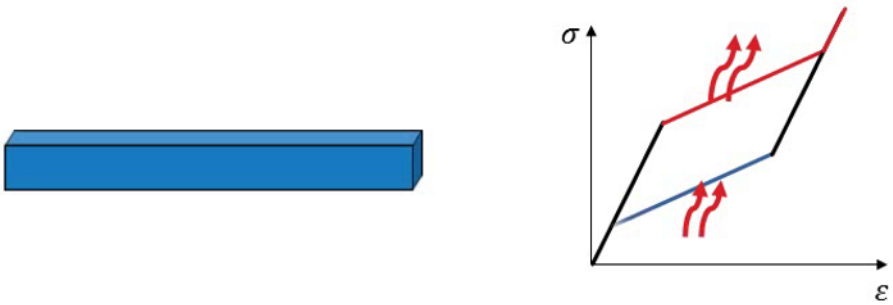

Figure 1 (Movie). Adiabatic phase transformation of an SMA sample. The adiabatic, exothermic phase transformation from austenite to martensite increases the SMA temperature and the endothermic transformation from martensite to austenite leads to a significant temperature decrease. (Right click to download this movie)

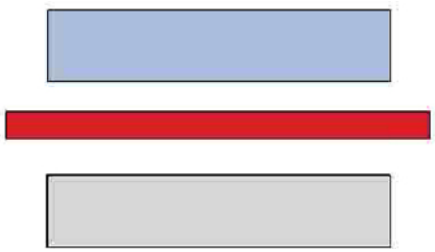

Figure 2 (Movie). Elastocaloric cooling cycle. The heat transfer between the heat source and the SMA take place at low temperature levels. In the next phase, the SMA is in a contact-free state and the fast (adiabatic) loading increases the SMA temperature. The subsequent heat transfer between the hot SMA and the heat sink take place at constant strain of the SMA. Upon completion of the heat transfer, fast adiabatic unloading leads to a significant temperature drop of the SMA. (Right click to download this movie)

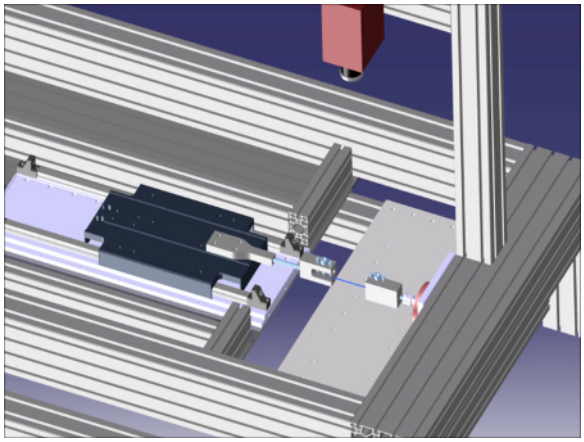

Figure 3 (Movie). 3D assembly animation. The animation shows the main components in the upper level of the test rig. (Right click to download this movie)

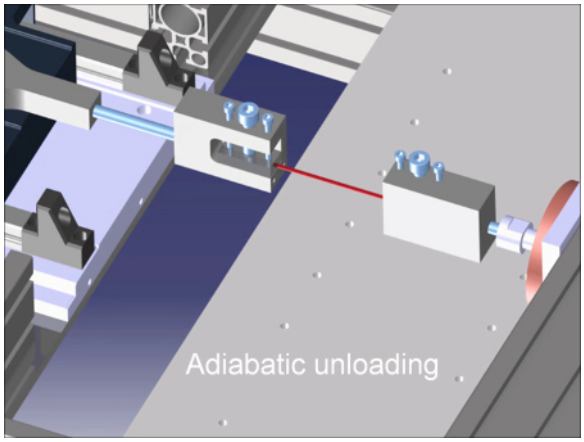

Figure 4 (Movie). 3D animation of the test rig. The animation shows an adiabatic loading and unloading cycle of the SMA. (Right click to download this movie)

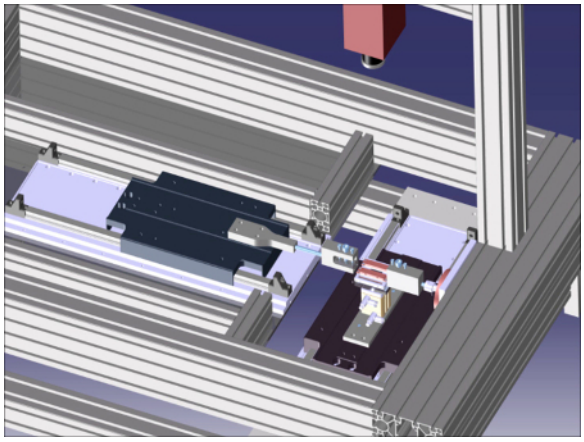

Figure 6 (Movie). 3D assembly animation. The animation shows the main components in the lower level of the test rig. (Right click to download this movie)

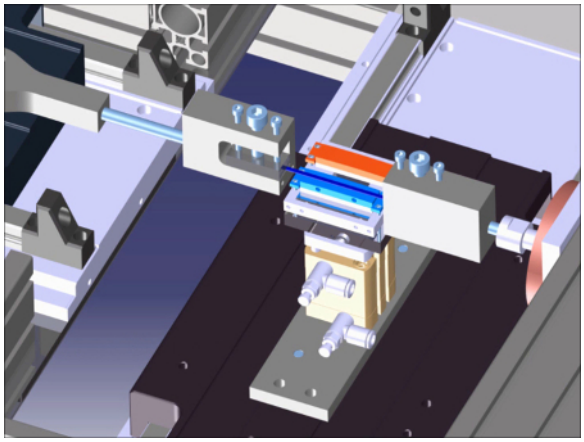

Figure 8 (Movie). 3D animation of the test rig. The animation shows an elastocaloric cooling cycle. (Right click to download this movie)

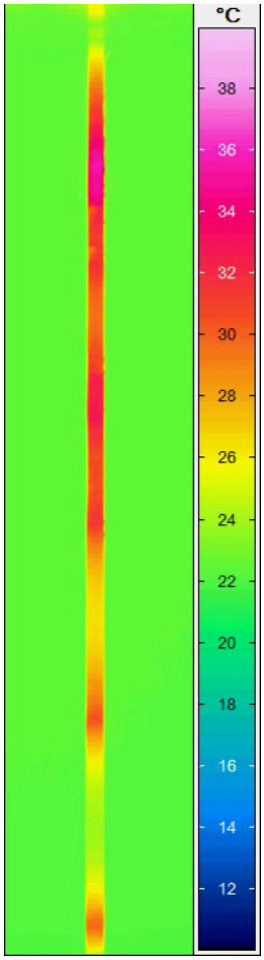

Movie 1. IR movie of the first three training cycles of a Ni-Ti ribbon at a strain rate of 1 x 10^{-3} sec^{-1} (5x playback rate). The IR movie shows an increasing homogenization effect of the elastocaloric effect by increasing number of training cycles. (Right click to download)

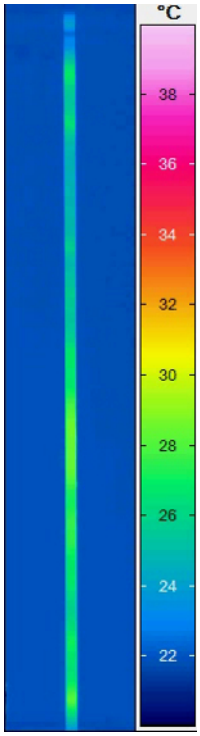

Movie 2. Mechanical loading of a NiTiCuV ribbon at a strain rate of 1 x 10^{-3} sec^{-1} (IR movie, 1x playback rate). The IR movie shows an inhomogeneous temperature distribution on the SMA surface. (Right click to download)

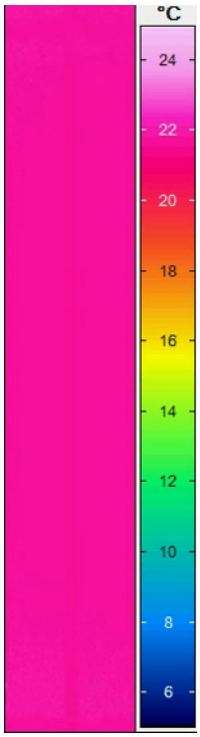

Movie 3. Mechanical unloading of a NiTiCuV ribbon at a strain rate of 1 x 10^{-3} sec^{-1} (IR movie; 1x playback rate). The IR movie shows an inhomogeneous temperature distribution on the SMA surface. (Right click to download)

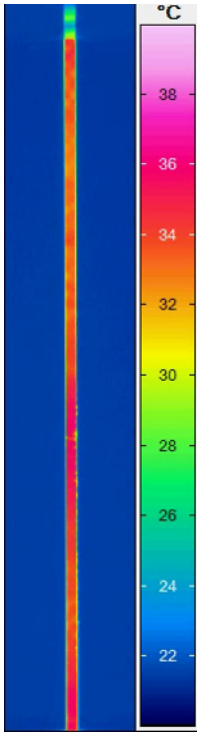

Movie 4. Mechanical loading of a NiTiCuV ribbon (A = 1.07 mm^2) at a strain rate of 1 x 10^{-1} sec^{-1} (IR movie, 10x slower playback rate). The IR movie shows a homogeneous temperature distribution on the SMA surface. (Right click to download)

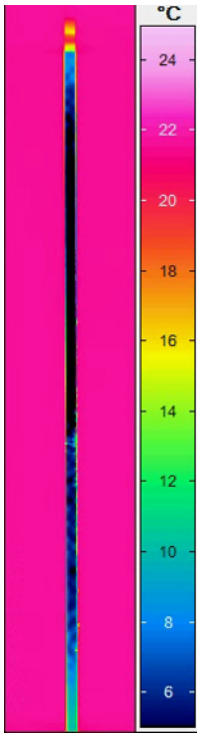

Movie 5. Mechanical unloading of a NiTiCuV ribbon at a strain rate of 1 x 10^{-1} sec^{-1} (IR movie, 10x slower playback rate). The IR movie shows a homogeneous temperature distribution on the SMA surface. (Right click to download)

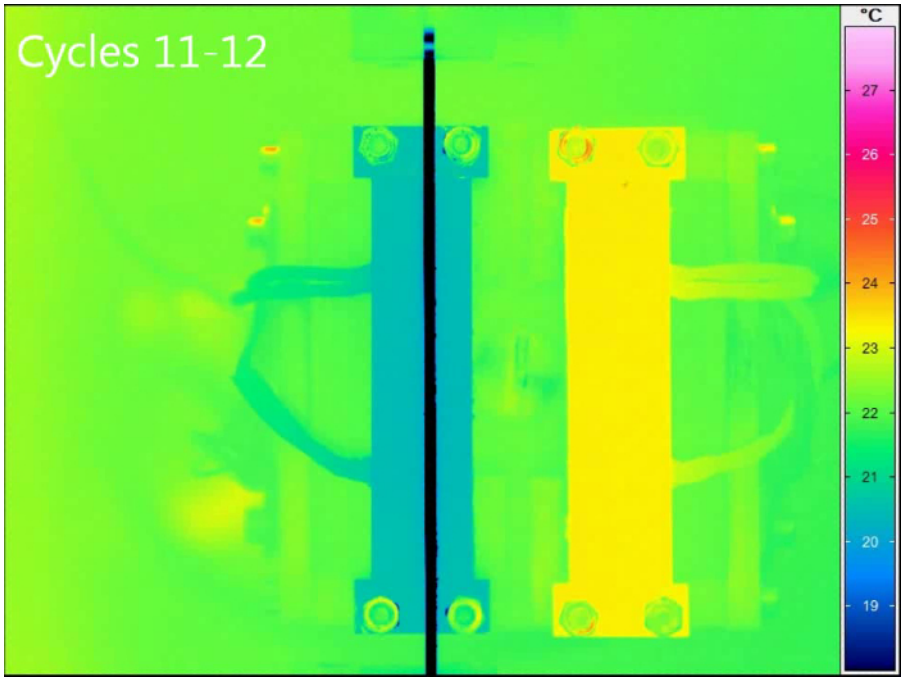

Movie 6. IR movie of a 40 cycle cooling process. The contact time between NiTiCuV sample and heat sink/source was set to 6 sec. The movie shows the cycles: 1, 2, 11, 12, 21, 22, 31, 32 and 40. (Right click to download)

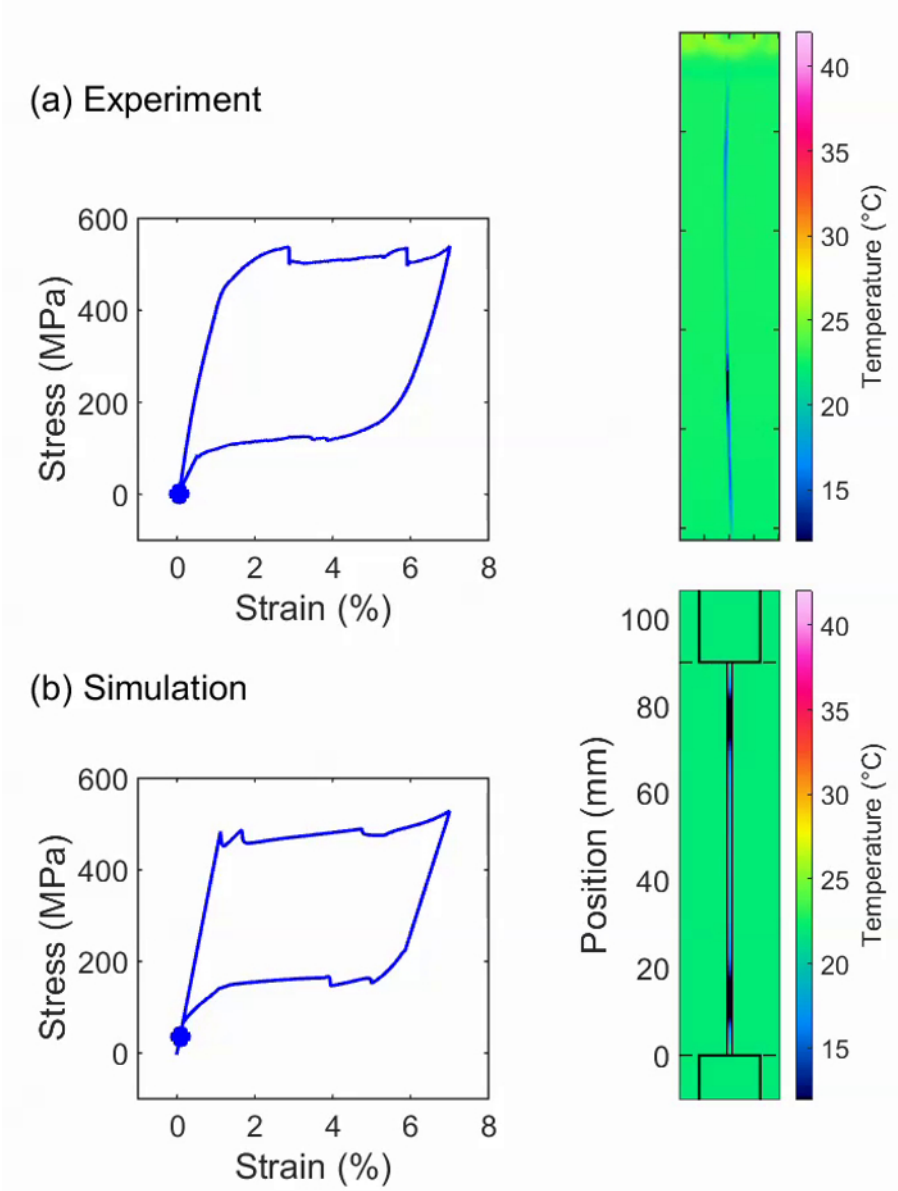

Movie 7. Comparison between experiment and simulation results of a Ni-Ti wire with a diameter of 0.6 mm (A = 0.2734 mm^2). The validation experiment is a tensile test at a strain rate of 1 x 10^{-3} sec^{-1}. The model is able to reproduce the mechanical and thermal material behavior and allows for a prediction of temperature fronts appearing during mechanical cycling. (Right click to download)

Discussion

The presented scientific test rig enables comprehensive investigation of elastocaloric materials and cooling processes by performing the experiments described in the protocol section. Precise alignment of the sample before clamping is crucial for all the experiments. Bad alignment can potentially lead to early material failure. Furthermore, the maximum applied strain has significant influence on the material lifetime, whereas the required strain to reach a complete phase transformation depends on the alloy composition. The transformation strain of the investigated NiTiCuV alloy (see **Figure 10**) is significantly lower than the transformation strain of the Ni-Ti alloy shown in **Figure 9** and **Figure 13**. To this end, initial tests to identify the transformation strain have to be performed for new alloys.

The development needs for the testing platform were the independent control of process parameters and the monitoring of thermal and mechanical behavior of the interacting process components (SMA sample, heat source and heat sink) during all cycle phases. Therefore, the heat sink and the heat source were mounted next to each other enabling simultaneous, thermographic measurements of the SMA sample and the heat source/sink during all process phases. The inhomogeneous temperature distribution on the SMA ribbon, as well as the influence of the temperature evolution of the heat sink and the heat source on the SMA behavior (see **Figure 10** and **Movie 6**), illustrate the need for the investigation of the thermographic process. The temperature profile and inhomogeneous heat exchange do not only affect the efficiency of the process; the material lifetime is also influenced by the temperature profile. High temperatures during mechanical cycling lead to a significant increase of functional and structural fatigue of the material [12-14]. However, long material lifetime is crucial for elastocaloric cooling devices which have to perform more than 1 x 10^6 cycles. In order to determine the temperature profile of the material by means of thermography, preliminary

experiments showed that a homogeneous, high emissivity coefficient of the material is required. The material coating (a high emissivity varnish) provides a more reproducible emissivity coefficient, independent of the alloy composition and the applied surface treatment of the samples. The investigation of the temperature distribution on a SMA ribbon with a length of 90 mm requires a resolution of approximately 80 µm/pixel to cover the complete sample length with 1,280 pixels. This limits the minimum sample width to 240 µm to ensure that at least one IR pixel is always completely covered by the sample. Smaller samples can be investigated with the IR camera in combination with the microscope lens, if the measurement of the temperature profile of the complete sample is not required. The microscope lens provides a resolution of 15 µm/pixel and enables the investigation of samples with a width of 45 µm.

The designed scientific test rig further enables the investigation of advanced elastocaloric cooling cycles. Non-adiabatic loading of the SMA in contact with the heat sink can reduce the maximum SMA temperature during the process, which increases the efficiency by reducing the hysteresis width. Furthermore, lower maximum SMA temperatures could potentially increase the material lifetime.

The representative results achieved by the scientific test rig showed that the testing platform allows for the investigation of various alloys with different dimensions and form factors. The maximum cross-section of the samples is limited to 1.8 mm^2. The limitation is based on the maximum continuous force of the linear direct drive of 1,200 N. The sample dimensions influence the process control, whereas the strain rates at which the samples transform adiabatically are primarily influenced by the surface to cross-section ratio. In addition, the contact time between the SMA and the heat source/sink has to be adapted to the sample dimensions in order to optimize efficiency and/or cooling power. A large surface to cross-section ratio decreases the cycle time and the opposite ratio leads to slower processes. The choice of the sample size, as well as the sample geometry, defines the operational frequency of a future elastocaloric cooling device and has to be adapted to the application requirements.

The optimization of elastocaloric cooling processes is required in order to establish a novel environmentally friendly cooling technology which can be a competitive alternative to the conventional vapor compression based process. The designed scientific test setup and the development of new alloys such as NiTiCu [26] and NiTiCuV are first steps in the development of an efficient cooling device. To the best knowledge of the authors, this scientific setup is the first system which allows the investigation of the elastocaloric properties of an SMA during solid-state based cooling processes by monitoring the temperature of the SMA and the heat source/sink during all process steps. A straight forward modification of the heat source/sink and the clamps allows for the investigation of the conductive heat transfer of the SMA with other form factors like grids and tubes. However, the scientific test rig has been developed from a scientific point-of-view, and provides the possibility of comprehensive material and process investigations for process and material optimizations instead of high system performance. Further steps are required in order to transfer the findings obtained with the scientific test setup to the design of an elastocaloric cooling device. In this context, the developed thermomechanically coupled model supports the development process simulating the cooling process at the device level.

Disclosures

The authors have nothing to disclose.

Acknowledgements

The authors would like to acknowledge the support of the DFG priority program 1599 "Caloric effects in ferroic materials: New concepts for cooling" (Projects: EG101/23-1, SCHU2217/2-1, SE704/2-1, EG101/29-2, SCH2217/3-2, SE704/2-2).

References

1. Fähler, S., Rößler, U. K., *et al.* Caloric effects in ferroic materials: New concepts for cooling. *Adv. Eng. Mater.* **14** (1-2), 10-19 (2012).
2. Moya, X., Defay, E., Heine, V., & Mathur, N. D. Too cool to work. *Nat. Phys.* **11** (3), 202-205 (2015).
3. Starkov, I. a., & Starkov, a. S. On the thermodynamic foundations of solid-state cooler based on multiferroic materials. *Int. J. Refrig.* **37**, 249-256 (2014).
4. Caloric Effects in Ferroic Materials: New Concepts for Cooling. at <http://www.ferroiccooling.de/> (2012).
5. Moya, X., Kar-Narayan, S., & Mathur, N. D. Caloric materials near ferroic phase transitions. *Nat. Mater.* **13** (5), 439-50 (2014).
6. Shaw, J. A., & Kyriakides, S. On the nucleation and propagation of phase transformation fronts in a NiTi alloy. *Acta Mater.* **45** (2), 683-700 (1997).
7. Chang, B.-C., Shaw, J. a., & Iadicola, M. a. Thermodynamics of Shape Memory Alloy Wire: Modeling, Experiments, and Application. *Contin. Mech. Thermodyn.* **18** (1-2), 83-118 (2006).
8. Cui, J., Wu, Y. M., *et al.* Demonstration of high efficiency elastocaloric cooling with large Delta T using NiTi wires. *Appl. Phys. Lett.* **101** (7) 073904 (2012).
9. Ossmer, H., Lambrecht, F., Gültig, M., Chluba, C., Quandt, E., & Kohl, M. Evolution of temperature profiles in TiNi films for elastocaloric cooling. *Acta Mater.* **81**, 9-20 (2014).
10. Ossmer, H., Chluba, C., Krevet, B., Quandt, E., Rohde, M., & Kohl, M. Elastocaloric cooling using shape memory alloy films. *J. Phys. Conf. Ser.* **476** (1), 012138 (2013).
11. Schmidt, M., Schütze, A., & Seelecke, S. Scientific test setup for investigation of shape memory alloy based elastocaloric cooling processes. *Int. J. Refrig.* **54**, 88-97 (2015).
12. Tobushi, H., Shimeno, Y., Hachisuka, T., & Tanaka, K. Influence of strain rate on superelastic properties of TiNi shape memory alloy. *Mech. Mater.* **30** (2), 141-150 (1998).
13. Miyazaki, S., Mizukoshi, K., Ueki, T., Sakuma, T., & Liu, Y. Fatigue life of Ti-50 at.% Ni and Ti-40Ni-10Cu (at.%) shape memory alloy wires. *Mater. Sci. Eng. A.* **273-275**, 658-663 (1999).
14. Olbricht, J., Yawny, A., Condò, A. M., Lovey, F. C., & Eggeler, G. The influence of temperature on the evolution of functional properties during pseudoelastic cycling of ultra fine grained NiTi. *Mater. Sci. Eng. A.* **481-482**, 142-145 (2008).

15. Tušek, J., Engelbrecht, K., Mikkelsen, L. P., & Pryds, N. Elastocaloric effect of Ni-Ti wire for application in a cooling device. *J. Appl. Phys.* **117** (12), 124901 (2015).
16. Zarnetta, R., Takahashi, R., *et al.* Identification of Quaternary Shape Memory Alloys with Near-Zero Thermal Hysteresis and Unprecedented Functional Stability. *Adv. Funct. Mater.* **20** (12), 1917-1923 (2010).
17. Schmidt, M., Ullrich, J., *et al.* Thermal Stabilization of NiTiCuV Shape Memory Alloys: Observations During Elastocaloric Training. *Shape Mem. Superelasticity.* (2015).
18. Höhne, G., Hemminger, W., & Flammersheim, H.-J. *Differential Scanning Calorimetry.* Springer-Verlag Berlin Heidelberg: (2003).
19. Heintze, O., & Seelecke, S. A coupled thermomechanical model for shape memory alloys-From single crystal to polycrystal. *Mater. Sci. Eng. A.* **481-482**, 389-394 (2008).
20. Furst, S. J., Crews, J. H., & Seelecke, S. Numerical and experimental analysis of inhomogeneities in SMA wires induced by thermal boundary conditions. *Contin. Mech. Thermodyn.* **24** (4-6), 485-504 (2012).
21. Shaw, J., & Kyriakides, S. Thermomechanical aspects of NiTi. *J. Mech. Phys. Solids.* **43** (8), 1243-1281 (1995).
22. Schmidt, M., Schütze, A., & Seelecke, S. Cooling Efficiencies of a NiTi-Based Cooling Process. *ASME 2013 Conf. Smart Mater. Adapt. Struct. Intell. Syst. Vol. 1 Dev. Charact. Multifunct. Mater. Model. Simul. Control Adapt. Syst. Integr. Syst. Des. Implement.* , V001T04A014 (2013).
23. Achenbach, M., & Müller, I. A MODEL FOR SHAPE MEMORY. *Le J. Phys. Colloq.* **43** (C4), C4-163-C4-167 (1982).
24. Müller, I., & Seelecke, S. Thermodynamic aspects of shape memory alloys. *Math. Comput. Model.* **34** (12-13), 1307-1355 (2001).
25. Ullrich, J., Schmidt, M., *et al.* Experimental Investigation and Numerical Simulation of the Mechanical and Thermal Behavior of a Superelastic Shape Memory Alloy Beam During Bending. *ASME 2014 Conf. Smart Mater. Adapt. Struct. Intell. Syst. Vol. 2 Mech. Behav. Act. Mater. Integr. Syst. Des. Implementation; Bioinspired Smart Mater. Syst. Energy Harvest.* , V002T02A013 (2014).
26. Bechtold, C., Chluba, C., Lima de Miranda, R., & Quandt, E. High cyclic stability of the elastocaloric effect in sputtered TiNiCu shape memory films. *Appl. Phys. Lett.* **101** (9), 091903 (2012).

